ADVANCED OPTICAL MATERIALS
www.advopticalmat.de

Sub-Picosecond Response Time of a Hybrid VO_2:Silicon Waveguide at 1550 nm

Kent A. Hallman, Kevin J. Miller, Andrey Baydin, Sharon M. Weiss, and Richard F. Haglund**

Hybrid material systems are a promising approach for extending the capabilities of silicon photonics. Given the weak electro-optic and thermo-optic effects in silicon, there is intense interest in integrating an ultrafast-switching phase-change material with a large refractive index contrast into the waveguide, such as vanadium dioxide (VO_2). It is well established that the phase transition in VO_2 thin films can be triggered by ultrafast, 800 nm laser pulses, and that pump-laser fluence is a critical determinant of the recovery time of thin films irradiated by femtosecond pulses. However, thin-film experiments are not reliable guides to a VO_2:Si system for all-optical, on-chip switching because of the differences in VO_2 optical constants in the telecommunication band, and the complex sample geometry and alignment issues in a waveguide geometry. This paper reports the first demonstration that the reversible, ultrafast photoinduced phase transition in VO_2 can achieve sub-picosecond response when small VO_2 volumes are integrated into a silicon waveguide as the active element. The result suggests that VO_2 can be pursued as a strong candidate for waveguide switching with sub-picosecond on-off times.

1. Introduction

Phase-change materials, such as vanadium dioxide (VO_2) and $Ge_2Sb_2Te_5$ glass, are attracting widespread attention due to large changes in their optical properties that can be initiated by optical excitation and leveraged to modulate the performance of on-chip components for silicon photonics.[1–5] For ultrafast optical switching, VO_2 has long been viewed as a promising candidate for integration with silicon photonics components. However, while experiments during the last decade have shown that VO_2 thin films can be optically switched from the insulating to the metallic state and then recover on a picosecond time scale at low pump fluences,[6–8] most experiments were carried out at pump wavelengths near 800 nm, and none directly incorporated VO_2 into a silicon waveguide. Moreover, ultrafast electron-diffraction studies comparing the photo-induced phase transition (PIPT) using near band-edge (2000 nm) excitation versus 800 nm pumping showed that the former requires half the enthalpy change of the latter,[8] consistent with the observed monotonic decrease in PIPT threshold as the pump-laser photon energy approaches the VO_2 band edge and suggesting that the transition can be driven in a low-fluence, athermal regime.[9] Hence, while prior work provides a rationale for integrating VO_2 into Si photonic components,[10–13] there is still no direct evidence that a femtosecond optical pulse at telecommunication frequencies traversing a hybrid VO_2:Si waveguide can be switched on and off at ultrafast time scales, less than 1 ps.

The incorporation of VO_2 into silicon waveguide geometries is relatively recent. The transmission modulation of a continuous-wave (CW) signal by heating a Si ring-resonator with a VO_2 patch on a small section of the ring first demonstrated the feasibility of using VO_2 as the active material on a silicon photonic component; while the steady-stating heating carried out in this experiment did not allow investigation of response time, a modulation depth exceeding 6 dB was shown.[10] Nanosecond all-optical switching of a CW laser beam at 1550 nm in both in-line Si waveguide modulators and ring resonators subsequently showed that the response time of VO_2 incorporated atop these silicon photonic components could track the pulse width of the 1064 nm out-of-plane nanosecond pump laser.[12] Most recently, optical switching of a CW 1550 nm signal beam in Si_3N_4 dual waveguides covered with a thin film of VO_2, by 140 fs pulses from an 80 MHz Ti:Sapphire oscillator at wavelengths between 800 to 1000 nm, demonstrated the feasibility of using an in-plane all-optical pumping scheme with pJ threshold switching energy; however, the "on-off" switching time was not measured.[14]

Here, we take a significant step forward in establishing the feasibility of Tbps on-chip optical switching using hybrid VO_2:Si

Dr. K. A. Hallman, Dr. A. Baydin
Department of Physics and Astronomy
Vanderbilt University
2301 Vanderbilt Place, Nashville, TN 37235, USA
E-mail: themaninthehall@gmail.com
Dr. K. J. Miller
Interdisciplinary Graduate Program in Materials Science
Vanderbilt University
2301 Vanderbilt Place, Nashville, TN 37235, USA
Prof. S. M. Weiss
Department of Electrical Engineering and Computer Science
Department of Physics and Astronomy
and Interdisciplinary Graduate Program in Materials Science
Vanderbilt University
2301 Vanderbilt Place, Nashville, TN 37235, USA
Prof. R. F. Haglund
Department of Physics and Astronomy and Interdisciplinary Graduate Program in Materials Science
Vanderbilt University
2301 Vanderbilt Place, Nashville, TN 37235, USA
E-mail: richard.haglund@vanderbilt.edu
The ORCID identification number(s) for the author(s) of this article can be found under https://doi.org/10.1002/adom.202001721.

DOI: 10.1002/adom.202001721

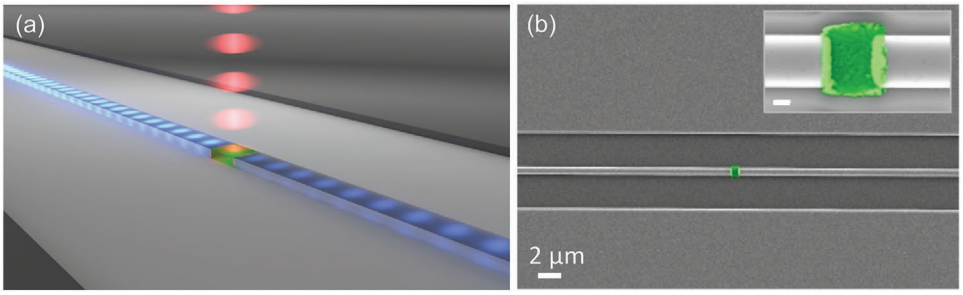

Figure 1. a) Schematic view of the pump-probe experiment, showing 1550 nm femtosecond pulses (bright blue) injected into the waveguide from the left and the gating femtosecond pulses (red) at 1670 nm illuminating the embedded VO_2 segment (green) from above. The attenuated pulses (faded blue) propagate to a detector (not shown). b) False color scanning-electron microscopy image of the embedded VO_2 modulator, 700 nm long; it is enlarged in the inset, where the scale bar is 200 nm.

photonic components by demonstrating record high-speed sub-picosecond response times in a silicon waveguide with an embedded section of VO_2. Importantly, unlike prior work, both the signal and pump beams are near 1550 nm. A 105 fs pulse (1550 nm), launched into a TE waveguide mode, is switched by a temporally synchronized 135 fs pulse (1670 nm) with "on-to-off" times below 1 ps at modest pump fluences. While the observed fluence dependence of the differential transmission is similar to pump-probe results on thin VO_2 films that show a transient metallic phase at low pump fluence and growth of a rutile metallic phase as high pump fluence,[6,15–18] there are additional complexities that must be considered in the optical dynamics of VO_2 when embedded in the spatially and thermally confined geometry of a waveguide despite the athermal nature of the low-fluence transition. In particular, the nonlinear dependence of the response time on pump fluence and on the injection geometry of the probe-beam indicates that incorporating a submicron length of VO_2 into a waveguide form factor creates a nonlinear material structure that has both design challenges and opportunities to optimize switching performance. Thus, this novel nonlinear optical material in a silicon waveguide geometry can drive significant progress in all-optical silicon photonics with its inherent advantages over all-electronic or electro-optic systems.

2. Experiment Layout and Procedure

Figure 1a illustrates the experimental concept: a train of femtosecond probe (signal) pulses at a pulse repetition frequency of 1 kHz (bright blue, 1550 nm), injected into one end of a silicon waveguide, is attenuated in a section of the waveguide filled by VO_2 (green) by pump pulses (red, 1670 nm) generated synchronously in the same optical parametric amplifier as the signal pulses. The transmitted, attenuated signal pulses (darker blue) are detected using a lock-in amplifier. Figure 1b shows one example of a hybrid VO_2:Si waveguide. The embedded VO_2 segment, 700 nm long, is located near the middle of a silicon waveguide about 3 mm long, as shown by the scanning electron microscopy image, where the embedded VO_2 segment is indicated in false color (green).

Figure 2 shows the experimental configuration in which the dynamical response of the waveguide was measured. An amplified titanium-sapphire laser system (Spectra Physics Spitfire Ace) producing nominal 100 fs pulses at 800 nm pumps an optical parametric amplifier (OPA, Light Conversion Topas) at 1 kHz repetition frequency. The OPA signal output is the probe beam that propagates through the waveguide; the idler output at 1670 nm is the free-space pump beam. A polarizing beam splitter separates the orthogonally polarized signal and

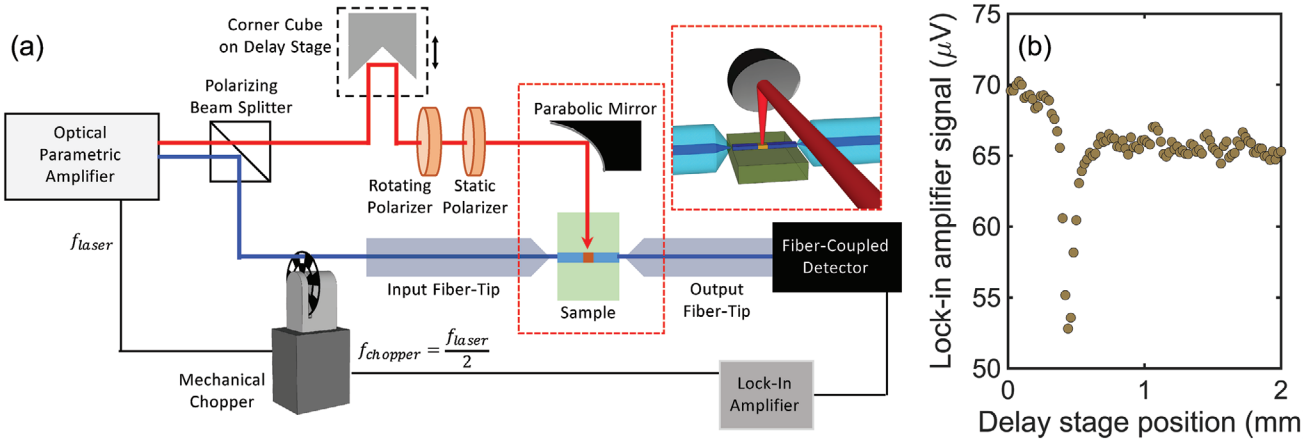

Figure 2. a) Experimental layout for the out-of-plane pump, in-waveguide probe configuration used to measure the temporal response of the embedded-VO_2 silicon waveguide. The inset shows a 3D perspective of the free-space geometry of the pump. b) The lock-in amplifier (LIA) trace corresponding to the optical data shown in Figure 3a. The delay-stage scan length between the FWHM points (≈0.2 mm) of the LIA trace corresponds to an optical pulse duration at the LIA of 0.64 ps.

Table 1. Probe and pump-beam characteristics.

	Probe beam	Pump beam
Wavelength	1550 nm	1670 nm
Repetition rate	500 Hz	1000 Hz
Pulse duration	105 fs	130 fs
Pulse energy	0.5 pJ[a)]	6–360 nJ
Beam diameter	220×700 nm^2	70 μm (e^{-2})
Insertion loss	10 dB	0
Fluence	33 μJ cm^{-2}[b)]	0.13–7.8 mJ cm^{-2}
Intensity	310 MW cm^{-2}[b)]	1–60 GW cm^{-2}

[a)]At input face of the waveguide; [b)]In the waveguide.

idler beams at the OPA output. The temporal duration of the pump and probe pulses are derived from a spectral scan of, and a Gaussian fit to, the OPA output, as described in Section S1 (Supporting Information). The characteristics of the pump and probe beams at the OPA output are summarized in **Table 1**.

The pump beam (red, Figure 2) is delayed with respect to the probe beam in a delay line comprising a corner cube on a computer-driven translation stage and focused onto the sample by a parabolic mirror. A pair of crossed polarizers on a computer-controlled rotation mount adjusts the fluence of the pump beam; to maintain the polarization of the pump beam fixed at the focusing mirror, only the upstream (laser side) polarizer is rotated, while the downstream polarizer remains fixed. The InGaAs detector for a pyroelectric power meter (not shown) on a flip mount in front of the parabolic mirror measures the average power of the pump beam, from which the energy per pulse and the fluence can be calculated.

The probe beam is chopped at 500 Hz, half the laser repetition rate, and this frequency provides the reference for phase-sensitive detection in the lock-in amplifier (LIA); the rationale for this configuration is discussed in Section S2 (Supporting Information). The input tapered fiber focuses the probe beam to a 2.5 μm spot and x–y–z piezoelectric actuators are adjusted to maximize the coupling of light from the tapered fiber into the proximal end facet of the silicon waveguide (220 nm × 700 nm). The average power coupled into the tapered fiber carrying the probe beam was estimated by exchanging the tapered fiber for an ordinary patch fiber connected to a fiber-coupled power meter. The insertion loss, estimated to be ≈10 dB, was confirmed by measuring the probe transmission through a waveguide without embedded VO_2 and is attributed, in part, to imperfect deposition of the VO_2 patch in the Si waveguide.[19]

The light transmitted through the VO_2 segment and onto the distal facet of the silicon waveguide is collected by the output tapered fiber, the alignment of which is controlled with similar piezoelectric actuators. Without further optical filtering or attenuation, the probe signal is then transmitted to a fiber-coupled indium gallium arsenide (InGaAs) detector (Thorlabs D400FC).

The pump beam is focused onto the VO_2 section by a parabolic mirror to avoid chromatic and spherical aberration. The pump-beam and parabolic-mirror axes must be parallel to guarantee that translating the mirror does not distort the shape of the beam spot, and negligible differences between measurements when the parabolic mirror is swept parallel and perpendicular to the waveguide axis justify the claim that the axes are appropriately aligned. The waist of the roughly Gaussian pump-beam focus—70 μm diameter at e^{-2} of peak intensity—was measured by blocking the probe, changing the LIA reference frequency to 1000 Hz, and translating the parabolic mirror so the beam spot was swept across the device. In this configuration, scattered pump light coupled into the waveguide was measured by the LIA as a function of beam spot (parabolic mirror) position and fit to a Gaussian distribution. Given the dimensions of the waveguide, this implies that when perfectly aligned, the fluence is essentially constant across the embedded VO_2. Information about the relevant optical properties of VO_2 are given in Section S3 (Supporting Information); relevant characteristics of the probe and pump beams are exhibited in Table 1.

It is important to note here that the pump beam illuminates a 35–40 μm segment of the silicon waveguide on either side of the VO_2 section. Since the threshold for nonlinear absorption in silicon pumped in the near IR is of order 2 cm GW^{-1},[20] one might be concerned about potential nonlinear effects on the probe-beam transmission in the silicon. However, studies of the nonlinear pulse propagation in silicon waveguides[21] and in silicon nanowires[22,23] confirm that nonlinear effects are totally negligible for such short lengths of silicon.

3. Experimental Results

Figure 3 shows the differential transmission [$-\Delta T/T$ (%)] as a function of pump-probe delay and illustrates the temporal switching behavior for the embedded-VO_2 silicon waveguides with a 700 nm long section of embedded VO_2. Figure 3a, acquired at a moderate pump fluence of 2.7 mJ cm^{-2}, shows that the duration of the signal pulse reaching the InGaAs detector is no more than 640 fs full width at half-maximum (FWHM). The pulse traces were fit by the sum of a Gaussian and a sigmoidal background.

Figure 3b shows the differential transmission for thirteen values of incident pump fluence, all acquired in a separate experiment and therefore under slightly different alignment conditions than the measurement in Figure 3a. The photo-induced switching exhibits three distinct responses: i) a low-fluence regime in which the signal returns to baseline in less than 1 ps (cool colors); ii) an intermediate-fluence response in which there is rapid switching, but an elevated background after switching is complete (earth tones); and iii) a high-fluence regime above roughly 5 mJ cm^{-2} in which the peak amplitude continues to rise sublinearly but the background after switching also rises (warm colors).

The rising background as one progressively increases fluence through these three regimes shows that an increasing, fluence-dependent fraction of the VO_2 is in the rutile crystallographic state, in contrast to data at the low end of the fluence range, where the signal recovers quickly to the initial background level. The rising background in (iii) indicates the onset of the increasing fraction of the VO_2 section to the rutile crystallographic state and the long relaxation time associated with rutile-to-monoclinic relaxation, consistent with experiments at 800 nm.[6]

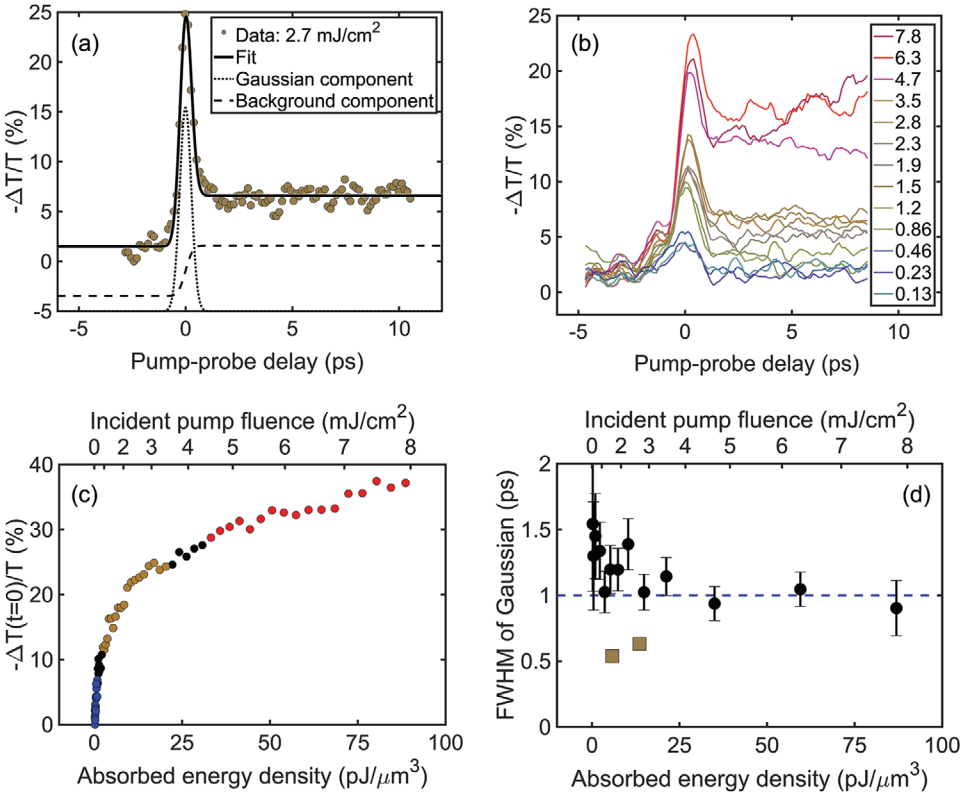

Figure 3. Differential transmission $-\Delta T/T$ (%) as a function of pump-probe delay a) for an incident pump fluence of 2.7 mJ cm^{-2} and b) for a range of incident pump fluences indicated by the legend on the right-hand side (units of mJ cm^{-2}), showing transition to the nearly fully switched rutile crystallographic phase at high fluences. The full width at half-maximum of the pump-probe response in (a) is 0.64 ps assuming a Gaussian temporal profile. Raw data for the curves in (b) were smoothed using a five-point moving average. c) Differential transmission versus incident pump fluence and absorbed energy density from below- to above-threshold levels for the monoclinic to rutile structural transformation, color-coded as in (b). d) Duration of the Gaussian component of the detected signal from the pump-probe measurements in (a) and (b), full-width at half-maximum (black circles). The error bars represent the 95% confidence intervals from the fits to all unsmoothed data from (b). The dashed blue line corresponds to a switching time of 1 ps. The brown square points were acquired at a different time than the black circle data, with adjusted alignment parameters. Error bars for these two points are smaller than the plotting symbols.

Figure 3c shows the differential transmission as a function of incident pump fluence at time $t = 0$, incorporating the data from Figure 3b as well as other experiments. Details of the calculation of the absorbed energy density are discussed in Section S4 (Supporting Information). From previous studies,[6] about 10 ps after the pump pulse, either reversion to the semiconducting phase or the structural phase transition and evolution to the rutile VO_2 phase begins to take place, depending on the fluence.

We calculated the FWHM duration of the Gaussian component of the pump-probe dynamics for the data in Figures 3a,b and 4 using the fitting procedure described in Section S5 (Supporting Information) and shown for the data in Figures 3a,b and 4 in Supporting Information Section S6.

The circular black data points in Figure 3d show that the FWHM signal duration corresponding to the differential transmission data in Figure 3b decreases monotonically to less than 1 ps as the pump fluence is increased, and is less than 1 ps at the highest fluences. The change in the pulse duration—not typically seen at all in thin-film experiments—is nonlinear and saturates as a function of pump fluence.

The brown square points in that same figure, corresponding to the transmission spectra in Figures 3a and 4d, were measured on a different day under different alignment conditions. In these two measurements, the "on-off" switching times are substantially shorter, of order 550–640 fs—and probably represent the shortest achievable switching times at near-optimal alignment for the intermediate-fluence regime. The difference between the two sets of measurements probably results from day-to-day variations in OPA tuning, alignment differences for the lensed fiber couplers to the waveguide, or spatial chirp at the input and output silicon waveguide facets due to variations in the interaction of the probe pulse with the lensed fiber tips. The fiber-to-waveguide alignment may be particularly sensitive to modest day-to-day variations because of contributions of the nonlinear refractive index in the mid-to-high range of pump fluences. (See Table S1 and accompanying text, Supporting Information.)

Figure 4 shows three pump-probe spectra selected from the measurements plotted in Figure 3b representing the modulator response at low, moderate and high pump fluences, as well as the pulse durations extracted for these spectra using the fitting procedure described in Section S6 (Supporting Information).

At the lowest pump fluences (see Figure 4a), the embedded VO_2 is just barely switched. The pulse duration thus reflects the

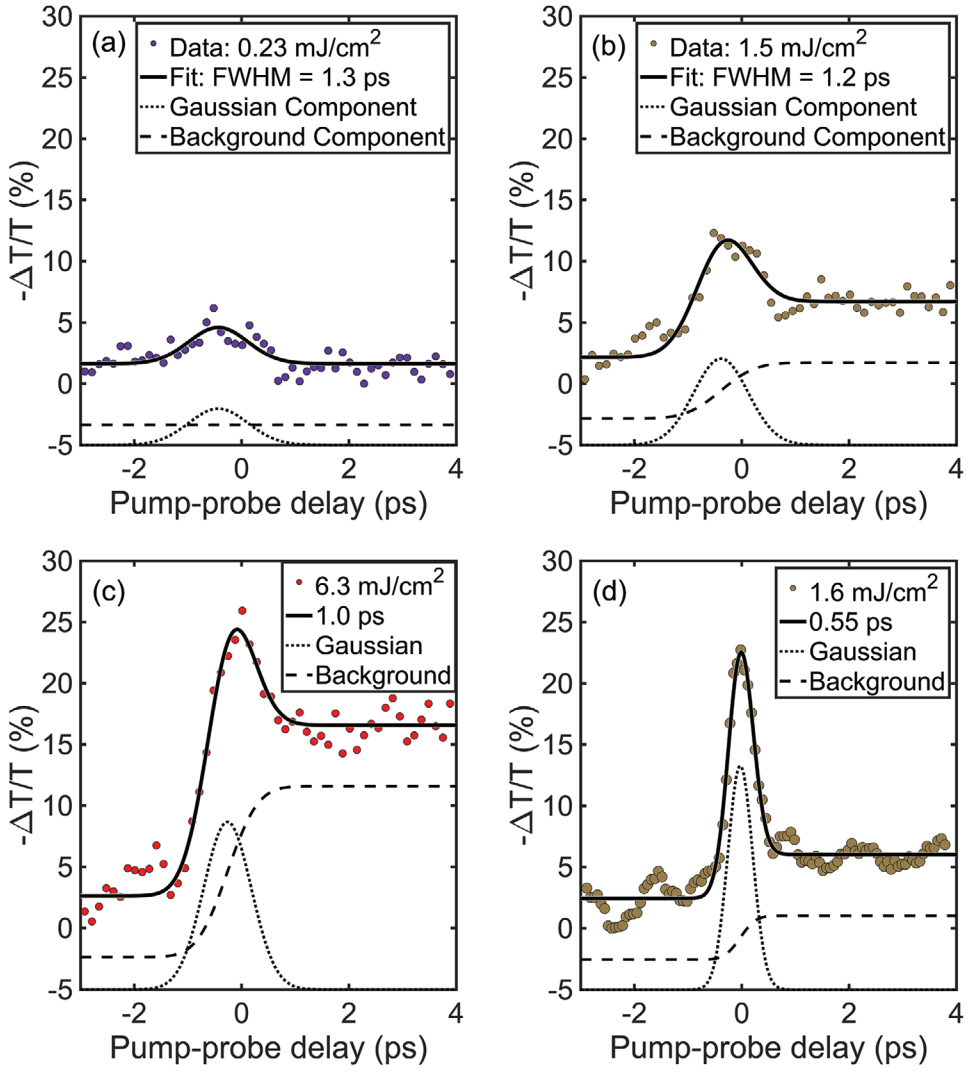

Figure 4. Differential transmission data (colored points) as a function of pump-probe delay, with fits to Gaussian pulse and background components for incident pump fluences of a) 0.23 mJ cm^{-2}, b) 1.2 mJ cm^{-2}, c) 6.3 mJ cm^{-2}, and d) 1.6 mJ cm^{-2}, derived from fits to data in Figure 3a,b. Data in (d) are collected on a different day with better alignment and are shown for comparison.

input probe pulse duration at the interface between waveguide and the embedded VO_2, and is dominated by the effects of dispersion in the input delivery fiber. Thus, the pulse duration reflected in the lock-in detector signal for Figure 4a can reasonably be considered to represent the instrumental response function. In Figure 4b, in the moderate fluence regime, one sees the sharp onset of the gating pulse, but also the hint of a long-term response that does not recover to background within 10 ps. In Figure 4c, the overall trend of rising background with increasing pump fluence is fully developed; and high background relative to the peak signal indicates substantial metallization of the VO_2 modulator—foreshadowing nanosecond recovery.

Figure 4d shows the differential transmission data for one of the brown square data in Figure 3d, acquired at a different time than the data in Figure 4a–c, which correspond to specific fluences in Figure 3b. The difference in pulse duration between the data of Figure 4b and Figure 4d is more than a factor 2, even though the data were acquired at the same pump fluence. Moreover, the contrast ratio is significantly higher for the pulse in Figure 4d—about a factor 2—due to the higher ratio of signal to background.

4. Discussion

Our experimental results are consistent with more than two decades of studies in which the ultrafast photo-induced phase transition (PIPT) in VO_2 has been explored for potential application to all-optical switching technologies.[24–27] The PIPT in VO_2 generates both an insulator-to-metal transition (IMT) and a monoclinic-to-rutile structural phase transition (SPT). Evidence from many experiments on thin films of VO_2[15–17,28] indicates that the IMT and SPT do not occur congruently, whether initiated by local heating[29] or by nanosecond laser.[12,30] Moreover, there is a critical threshold pump fluence above which the

rutile phase nucleates and grows,[6] and from which relaxation to the initial monoclinic crystal structure takes a few nanoseconds. Below this threshold, however, a transient metallic phase is observed that results from a coherent phonon excitation, which creates an excited electronic state that is not representative of the equilibrium nuclear positions *in either the semiconducting monoclinic or metallic rutile phases*. These observations are inconsistent with a purely thermal process. This transient sub-threshold phase has been observed in VO_2 thin films in time-dependent reflectivity,[15,16] transmissivity,[6] THz conductivity[26,27] and photoelectron spectroscopy;[31] the self-trapped-exciton-like excited state relaxes to near initial conditions on a time scale of a 2–5 ps.

In a conventional pump-probe experiment, the pump and probe pulses have roughly the same duration, and the probe pulse is focused in a small fraction of the area illuminated by the pump to ensure that boundary effects do not distort the probe signal. However, the experiment reported here differs from conventional pump-probe studies in significant ways:

1. Assuming that the input tapered fiber has a dispersion of 15 ps km^{-1} nm^{-1} typical of fused silica, the 105 fs signal pulse from the OPA is stretched to a duration of about 1.2 ps FWHM at the waveguide input, as measured in Figure 4a for the lowest pumping fluence.
2. The transit time for a point on the phase front of a probe pulse to pass through the 700 nm VO_2 section is of order 10 fs, negligible compared to probe-pulse duration, thus ...
3. ... the nonlinear absorption of the probe induced by the 135 fs pump pulse occurs during a small fraction of the probe-pulse duration as it traverses the embedded VO_2 segment.
4. The geometry of the VO_2 in this experiment is severely constrained compared to pump-probe studies on bulk thin films,[6,15] with typical focal-spot volumes more than a thousand times greater than the volume of VO_2 in the waveguide.

Against this background, we interpret the data in Figures 3 and 4 as follows. The linear absorption coefficient for monoclinic VO_2 over the spectral range spanned by pump and probe beams (Supporting Information, Section 1) is nearly constant, at $\alpha_0 = 2\ \mu m^{-1}$; absorption in the rutile phase is roughly an order of magnitude larger. The embedded VO_2 functions as an ultrafast absorptive modulator activated by the pump pulse. Because of the short pump-pulse duration, the absorption $-\Delta T/T$ rises rapidly to its peak; the initial slope of the pump-probe signal steepens with increasing fluence due to third-order nonlinear absorption. Even for pump fluences as low as 1 mJ cm^{-2}, the nonlinear absorption—at 800 nm equal to $\beta = 270 \pm 30$ cm GW^{-1} [32]—already exceeds $0.1\alpha_0$. Moreover, the probe pulse experiences this nearly instantaneous nonlinear absorptive effect—which enhances the total absorption exponentially—throughout the entire 700 nm segment of VO_2.

With increasing fluence, the conduction-band electron concentration increases from 10^{20} cm^{-3}, and the fraction of unit cells excited in the embedded VO_2 begins to increase beyond the roughly 0.1 required for cooperative nucleation of the rutile phase;[9] significant metallization—and subsequent growth of the rutile phase—begins, leading to a rising background with increasing fluence, indicated by sigmoidal dashed curves that appear in the fits. The hot electrons and initially cold monoclinic lattice then equilibrate in a mixed rutile-monoclinic phase on a picosecond time scale.[16]

Measurements on VO_2 thin films excited by femtosecond pulses at 800 nm have shown that there is a fast-recovering metallic monoclinic transition that recovers on the time scale of a few picoseconds for incident fluences below 1–2 mJ cm^{-2}; as fluence rises from 1 to 5 mJ cm^{-2}, the post-switch background relaxes on an increasingly long timescale. This behavior also appears in thin films undergoing the ultrafast PIPT across a wide range of lattice mismatches and spatial correlation lengths.[6] This same behavior is evident in Figures 3a,b and 4b,c: for incident fluences below 3 mJ cm^{-2} the background signal returns close to baseline within the 10 ps measurement window, showing that at these fluences the VO_2 remains largely in the monoclinic phase[7,17,28] after the transient metallization phase.

The implications of these results for the present experiment are that 1) at an incident fluences of 1–3 mJ cm^{-2}, the embedded VO_2 has been only partially transformed from the monoclinic to the rutile crystalline phase, slightly slowing relaxation to the initial state; 2) the maximum value of contrast ratio between "on" and "off" states of the VO_2 will be reached near this threshold (see Figure 3d); and 3) because this threshold electron density is reached by the end of the 135 fs pump pulse, we expect that the maximum probe-pulse signal also reaches the detector not long after the pump pulse is over because at that point the absorbing rutile phase is well formed.

Moreover, the VO_2 section is thermally isolated by the SiO_2 substrate, and thus sheds the absorbed pump energy only very slowly by diffusive transport to the silicon waveguide. Given the confined geometry of the waveguide and the interface with the embedded VO_2, boundary effects on the waveguide and the substrate probably constrain the recovery time for the PIPT to the nanosecond time scale. The rising postswitch background beyond 4 ps for the higher fluences observed in this experiment would clearly be problematic for high modulator frequencies, because above the intermediate fluence range, so much of the embedded VO_2 transforms to the rutile crystalline phase that recovery to the initial state takes nanoseconds or longer—thus posing a critical obstacle to switching faster than a few GHz. This residual signal is almost certainly due to the pump beam, as the probe fluence—33 μJ cm^{-2}—is not sufficient to initiate substantial metallization of the VO_2 at ambient temperature.[27]

Nonlinear pump-pulse effects on the silicon waveguide can be ruled out. Given the measured two-photon absorption $\beta_T \approx 0.5$ cm GW^{-1} and nonlinear index $n_2 \approx 2.8 \times 10^{-5}$ cm^2 GW^{-1} for silicon at 1670 nm,[20] the fractional change in absorptive and refractive properties of silicon even at the highest intensities in this experiment is of order 10^{-4}. This also rules out free-carrier absorption effects; the small change in $-\Delta T/T$ signal at the lowest fluence (see Figure 4a) is due solely to the low density of electronic excitation. Furthermore, by translating the pump-beam spot from the hybrid waveguide to a silicon waveguide on the same chip, we found that there was no change in the measured probe signal at the pump fluences employed.

Perhaps surprisingly, the dynamics for the 1670 nm pump–1550 nm probe sequence resemble those observed in optical pump (800 nm)–(white-light) probe experiments;[15,16] in the latter, with pump–photon energies twice the bandgap energy

of VO_2, one expects to generate a substantial population of hot phonons that heat the VO_2 as they cascade down the ladder of excited states. In fact, however, the observed kinetics are also quite consistent with the pump-wavelength dependence at 2000 nm reported by Tao et al.:[8] in the high-fluence regime here—where the transformation to the rutile phase is nearly complete—the measured values for the switching energy are of order 0.6 eV nm^{-3}, within a factor two of the value 1 eV nm^{-3} measured in the ultrafast electron-diffraction experiment.

Therefore, the nonequilibrium dynamics of the photo-induced phase transition in even this simple in-line structure poses significant questions still to be resolved. The VO_2 fluence-versus-substrate temperature phase diagram proposed by Cocker et al. based on optical pump-THz probe measurements on thin VO_2 films on *a*-cut sapphire substrates suggests that substrate temperature plays a crucial role in ameliorating the evolution of the rutile crystalline phase and permitting picosecond relaxation. Consistent with the present results, the phase diagram shows that at room temperature and even at incident fluences as low as 1.5 mJ cm^{-2}, the crystallographic phase transition begins to nucleate and convert a fraction of the illuminated volume into the metallic phase with its long relaxation time; at fluences of 8 mJ cm^{-2}, in fact, the entire pumped volume of the film transitions immediately into the rutile phase.[33] But at 225 K substrate temperature, picosecond relaxation to background is observed even for fluences approaching 4 mJ cm^{-2}. That temperature range could be reached by thermoelectric cooling—thus enabling the optimal ultrafast dynamics at higher fluence, albeit at the cost of modest additional power consumption. Better overall thermal management might also be achieved by building this in-line waveguide switch on a silicon-on-sapphire (SOS) substrate that would have better thermal diffusivity away from the pumped VO_2 waveguide segment. The magnitude of the thermal loading from a single pulse and repetitive switching are estimated in Section S4 (Supporting Information), and are found to be much smaller than necessary to drive the phase transition.

Finally, it should be noted that the issue of lifetime of VO_2 switching performance at high pulse repetition frequency is obviously a critical one. The longest life-cycle tests in the literature are for thin-film VO_2 microwave switches, which have shown of order $250 \cdot 10^6$ switching cycles without degradation in performance.[34] Experiments on our device carried out over several months reached a similar level of switching longevity without any evidence of degradation. Recently switching rates in microwave circuits employing VO_2 as a modulating element have been tested at repetition rates up to a few tens of GHz, which show a modest decrease in switching contrast above 10 GHz.[5] However, these are tests employing electrical switching that in principle cost a good deal more energy per switch, have intrinsically longer switching times and potentially alter the VO_2 characteristics at a more rapid rate than the photo-induced phase transition with its low energy input.

5. Conclusions

The results presented in Figures 3 and 4 show the first experimental demonstration of a sub-picosecond response time for a small block of VO_2 embedded in a Si waveguide driven by the VO_2 insulator-to-metal phase transition to switch between insulating and metallic states while embedded in a Si waveguide. The transmission intensity of an ultrafast 1550 nm probe pulse propagating in the waveguide was modulated by another femtosecond pulse incident on the VO_2 patch with a maximum transmission contrast of about 22%. Response times as short as 0.55 ps were measured at modest pump fluences, and are probably close to the absolute limits for this in-line absorption waveguide switch configuration. The dispersion-lengthened duration of the input pulse, which is injected into the waveguide by a tapered silica fiber, does not appear to be the fundamental limiting factor in the performance of the in-line modulator. Thus, for the in-line hybrid waveguide, the pursuit of substantial reductions in switching time is now less urgent than optimizing the size, shape and volume of the VO_2 structure, as well as addressing the thermal management of the chip at high pump rates. Implementation of extant on-chip, in-plane optical pumping designs[35,36] and investigation of alternate optical-switching geometries such as resonant and interferometric configurations offer significant opportunities to make further progress toward practical implementation of a hybrid VO_2:Si all-optical switch.

6. Experimental Methods

Device Fabrication: Silicon waveguides with embedded VO_2 sections (green segment in Figure 1) were fabricated on silicon-on-insulator wafers (220 nm device layer, 3 µm buried oxide layer, SOITEC) using standard lithographic procedures.[19] Silicon waveguides with 700 nm gaps and widths of 700 nm were defined by electron beam lithography (JEOL 9300FS-100kV) and subsequent reactive ion etching using a C_4F_8/SF_6/Ar gas mixture (Oxford Plasmalab 100). A second round of electron-beam lithography (Raith eLine) opened windows over the gaps in the waveguides for the VO_2 deposition. Then, VO_x was deposited at room temperature by RF magnetron sputtering of vanadium metal at 6 mTorr total pressure with 20 sccm Ar and 1 sccm O_2.[37]

After lift-off, the devices were annealed for 7 min at 450 °C in 250 mTorr of O_2 to form polycrystalline VO_2 sections in the waveguide gaps. The complete VO_2 lithography, deposition, liftoff, and annealing process was performed in two identical iterations to ensure complete O_2 diffusion during the anneal step. Atomic-force microscope (AFM) measurements on similarly prepared samples suggested that the average thickness of the VO_2 over the 700 nm-long waveguide gap was ≈150 nm compared to the waveguide height of 220 nm.[19] All waveguides were cleaved to allow access for input and output butt-coupled tapered fibers (OZ Optics). The postcleaved devices measured ≈3 mm in overall length.

Supporting Information

Supporting Information is available from the Wiley Online Library or from the author.

Acknowledgements

This research was supported in part by the National Science Foundation (grant EECS 1509740). The authors thank Dr. Sergey Avanesyan (Fisk University) for help in resolving issues relating to the pump-probe optical-delay line, Prof. Norman Tolk for making the optical parametric

amplifier system available for these experiments, and Francis Afzal for the concept drawing in Figure 1a. Silicon waveguides were fabricated at the Center for Nanophase Materials Sciences, a DOE Office of Science User Facility. Selective VO_2 deposition and SEM imaging were carried out at the Vanderbilt Institute of Nanoscale Science and Engineering.

Conflict of Interest

The authors declare no conflict of interest.

Keywords

differential transmission, phase change, response time, silicon photonics, vanadium dioxide

Received: October 7, 2020
Revised: November 9, 2020
Published online: December 4, 2020

[1] K. J. Miller, R. F. Haglund, S. M. Weiss, *Opt. Mater. Express* **2018**, *8*, 2415.
[2] M. Wuttig, H. Bhaskaran, T. Taubner, *Nat. Photonics* **2017**, *11*, 465.
[3] J. J. Zheng, A. Khanolkar, P. P. Xu, S. Deshmukh, J. Myers, J. Frantz, E. Pop, J. Hendrickson, J. Doylend, N. Boechler, A. Majumdar, *Opt. Mater. Express* **2018**, *8*, 2017,.
[4] C. M. Wu, H. S. Yu, H. Li, X. H. Zhang, I. Takeuchi, M. Li, *ACS Photonics* **2019**, *6*, 87.
[5] S. D. Ha, Y. Zhou, C. J. Fisher, S. Ramanathan, J. P. Treadway, *J. Appl. Phys.* **2013**, *113*, 184501.
[6] N. F. Brady, K. Appavoo, M. Seo, J. Nag, R. P. Prasankumar, R. F. Haglund, D. J. Hilton, *J. Phys.: Condens. Matter* **2016**, *28*, 125603.
[7] D. Wegkamp, M. Herzog, L. Xian, M. Gatti, P. Cudazzo, C. L. McGahan, R. E. Marvel, R. F. Haglund Jr., A. Rubio, J. Stähler, M. Wolf, *Phys. Rev. Lett.* **2014**, *113*, 216401.
[8] Z. S. Tao, F. R. Zhou, T. R. T. Han, D. Torres, T. Y. Wang, N. Sepulveda, K. Chang, M. Young, R. R. Lunt, C. Y. Ruan, *Sci. Rep.* **2016**, *6*, 38514.
[9] M. Rini, Z. Hao, R. W. Schoenlein, C. Giannetti, F. Parmigiani, S. Fourmaux, J. C. Kieffer, A. Fujimori, M. Onoda, S. Wall, A. Cavalleri, *Appl. Phys. Lett.* **2008**, *92*, 181904.
[10] R. M. Briggs, I. M. Pryce, H. A. Atwater, *Opt. Express* **2010**, *18*, 11192.
[11] P. Markov, R. E. Marvel, H. J. Conley, K. J. Miller, R. F. Haglund, S. M. Weiss, *ACS Photonics* **2015**, *2*, 1175.
[12] J. D. Ryckman, K. A. Hallman, R. E. Marvel, R. F. Haglund, S. M. Weiss, *Opt. Express* **2013**, *21*, 10753.
[13] A. Joushaghani, J. Jeong, S. Paradis, D. Alain, J. S. Aitchison, J. K. S. Poon, *Opt. Express* **2015**, *23*, 3657.
[14] H. M. K. Wong, Z. Yan, K. A. Hallman, R. E. Marvel, R. P. Prasankumar, R. F. Haglund, A. S. Helmy, *ACS Photonics* **2019**, *6*, 2734.
[15] S. Wall, D. Wegkamp, L. Foglia, K. Appavoo, J. Nag, R. F. Haglund, J. Stähler, M. Wolf, *Nat. Commun.* **2012**, *3*, 721.
[16] S. Wall, L. Foglia, D. Wegkamp, K. Appavoo, J. Nag, R. F. Haglund, J. Stähler, M. Wolf, *Phys. Rev. B* **2013**, *87*, 115126.
[17] V. R. Morrison, R. P. Chatelain, K. L. Tiwari, A. Hendaoui, A. Bruhacs, M. Chaker, B. J. Siwick, *Science* **2014**, *346*, 445.
[18] M. R. Otto, L. P. R. de Cotret, D. A. Valverde-Chavez, K. L. Tiwari, N. Emond, M. Chaker, D. G. Cooke, B. J. Siwick, *Proc. Natl. Acad. Sci. USA* **2019**, *116*, 450.
[19] K. J. Miller, K. A. Hallman, R. F. Haglund, S. M. Weiss, *Opt. Express* **2017**, *25*, 26527.
[20] Q. Lin, J. Zhang, G. Piredda, R. W. Boyd, P. M. Fauchet, G. P. Agrawal, *Appl. Phys. Lett.* **2007**, *91*, 021111.
[21] H. K. Tsang, C. S. Wong, T. K. Liang, I. E. Day, S. W. Roberts, A. Harpin, J. Drake, M. Asghari, *Appl. Phys. Lett.* **2002**, *80*, 416.
[22] E. Dulkeith, Y. A. Vlasov, X. G. Chen, N. C. Panoiu, R. M. Osgood, *Opt. Express* **2006**, *14*, 5524.
[23] E. Dulkeith, F. N. Xia, L. Schares, W. M. J. Green, Y. A. Vlasov, *Opt. Express* **2006**, *14*, 3853.
[24] M. F. Becker, A. B. Buckman, R. M. Walser, T. Lepine, P. Georges, A. Brun, *Appl. Phys. Lett.* **1994**, *65*, 1507.
[25] M. F. Becker, A. B. Buckman, R. M. Walser, T. Lepine, P. Georges, A. Brun, *J. Appl. Phys.* **1996**, *79*, 2404.
[26] C. Kübler, H. Ehrke, R. Huber, R. Lopez, A. Halabica, R. F. Haglund, A. Leitenstorfer, *Phys. Rev. Lett.* **2007**, *99*, 116401.
[27] A. Pashkin, C. Kübler, H. Ehrke, R. Lopez, A. Halabica, R. F. Haglund, R. Huber, A. Leitenstorfer, *Phys. Rev. B* **2011**, *83*, 195120.
[28] Z. S. Tao, T. R. T. Han, S. D. Mahanti, P. M. Duxbury, F. Yuan, C. Y. Ruan, K. Wang, J. Q. Wu, *Phys. Rev. Lett.* **2012**, *109*, 166406.
[29] J. Nag, R. F. Haglund, E. A. Payzant, K. L. More, *J. Appl. Phys.* **2012**, *112*, 103532.
[30] J. Laverock, S. Kittiwatanakul, A. A. Zakharov, Y. R. Niu, B. Chen, S. A. Wolf, J. W. Lu, K. E. Smith, *Phys. Rev. Lett.* **2014**, *113*, 216402.
[31] K. Appavoo, B. Wang, N. F. Brady, M. Seo, J. Nag, R. P. Prasankumar, D. J. Hilton, S. T. Pantelides, R. F. Haglund, *Nano Lett.* **2014**, *14*, 1127.
[32] R. Lopez, R. F. Haglund, L. C. Feldman, L. A. Boatner, T. E. Haynes, *Appl. Phys. Lett.* **2004**, *85*, 5191.
[33] T. L. Cocker, L. V. Titova, S. Fourmaux, G. Holloway, H. C. Bandulet, D. Brassard, J. C. Kieffer, M. A. El Khakani, F. A. Hegmann, *Phys. Rev. B* **2012**, *85*, 155120.
[34] A. Crunteanu, J. Givernaud, J. Leroy, D. Mardivirin, C. Champeaux, J. C. Orlianges, A. Catherinot, P. Blondy, *Sci. Technol. Adv. Mater.* **2010**, *11*, 065002 .
[35] P. Markov, J. G. Valentine, S. M. Weiss, *Opt. Express* **2012**, *20*, 14705.
[36] T. Barwicz, T. W. Lichoulas, Y. Taira, Y. Martin, S. Takenobu, A. Janta-Polczynski, H. Numata, E. L. Kimbrell, J. W. Nah, B. Peng, D. Childers, R. Leidy, M. Khater, S. Kamlapurkar, E. Cyr, S. Engelmann, P. Fortier, N. Boyer, *Opt. Fiber Technol.* **2018**, *44*, 24.
[37] R. E. Marvel, R. R. Harl, V. Craciun, B. R. Rogers, R. F. Haglund, *Acta Mater.* **2015**, *91*, 217.

